ACS APPLIED BIO MATERIALS

www.acsabm.org Article

Triphenylamine-Naphthalimide-Based "On−Off−On" AIEgen for Imaging Golgi Apparatus and Endoplasmic Reticulum

Phanindra Kumar,[‡] Tripti Mishra,[‡] Sanyam, Anirban Mondal,* and Sudipta Basu*

Cite This: https://doi.org/10.1021/acsabm.4c01722 Read Online

ACCESS | Metrics & More | Article Recommendations | Supporting Information

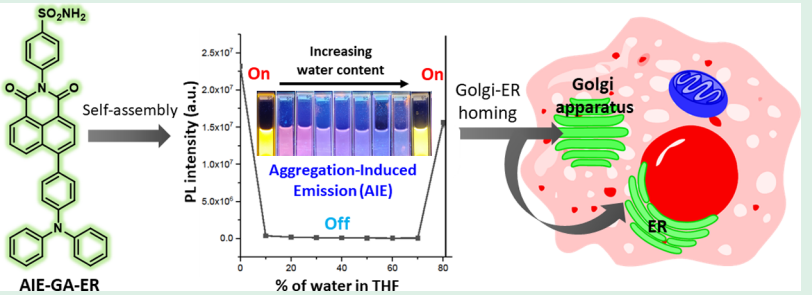

ABSTRACT: Golgi apparatus (GA) and endoplasmic reticulum (ER) are two of the interesting subcellular organelles that are critical for protein synthesis, folding, processing, post-translational modifications, and secretion. Consequently, dysregulation in GA and ER and cross-talk between them are implicated in numerous diseases including cancer. As a result, simultaneous visualization of the GA and ER in cancer cells is extremely crucial for developing cancer therapeutics. To address this, herein, we have designed and synthesized a 1,8-napthalimide-based small molecule (AIE-GA-ER) consisting of phenylsulfonamide as Golgi-ER homing and triphenylamine-napthalimide as aggregation-induced emission (AIE) triggering moieties. AIE-GA-ER exhibited remarkable "on−off−on" AIE properties in THF/water binary solvent system due to aggregated "on-state" in pure THF and 80% water in THF. Molecular dynamic simulations and density functional theory (DFT) calculations exhibited the underlying mechanism of the emissive property of AIE-GA-ER to be the interplay between intramolecular charge transfer (ICT) stabilization and aggregation in THF, DMSO, and water. AIE-GA-ER efficiently homed into the GA and ER of HCT-116 colon cancer cells within 15−30 min as well as noncancerous human retinal epithelial pigment cells (RPE-1) within 3 h with minimum toxicity. This AIEgen has the potential to illuminate the Golgi apparatus and ER simultaneously in cancer cells to understand the chemical biology of their cross-talk for next-generation cancer therapeutics.

KEYWORDS: *Golgi apparatus, endoplasmic reticulum, aggregation-induced-emission, internal charge transfer, molecular simulations, density functional theory*

INTRODUCTION

The Golgi apparatus (GA) and endoplasmic reticulum (ER) are two vital subcellular organelles responsible for a wide range of biological functions, including protein synthesis, folding, accumulation, processing, sorting, and secretion, as well as maintaining ion homeostasis, responding to stress, and regulating apoptosis.[1−10] Given their central role, any disruption in the structure or function of the GA and ER can lead to various pathological conditions, including cancer.[11−21] Moreover, to make the scenario even more complicated, cross-talk between GA and ER is implicated in cancer progression, hence emerging as a future target for anticancer therapy.[22−24] Therefore, simultaneous visualization of GA and ER in disease states like cancer is crucial for advancing the development of novel Golgi-ER-targeted cancer therapies.[25−34] In this context, small-molecule-aggregation-induced emitters (AIEgens) have shown great promise for imaging biomolecules, offering new avenues for research and treatment.

In recent decades, aggregation-induced emission active probes (AIEgens) have emerged as vital tools for biomedical imaging, celebrated for their brilliant luminescence and exceptional photostability.[35−40] These small molecule AIEgens have been extensively utilized to illuminate various subcellular organelles, including mitochondria, lysosomes, and lipid droplets, particularly in theranostic applications.[41−48] However, despite their remarkable potential, the development of small molecule AIEgens specifically for imaging the Golgi

Received: November 16, 2024
Revised: January 6, 2025
Accepted: January 10, 2025

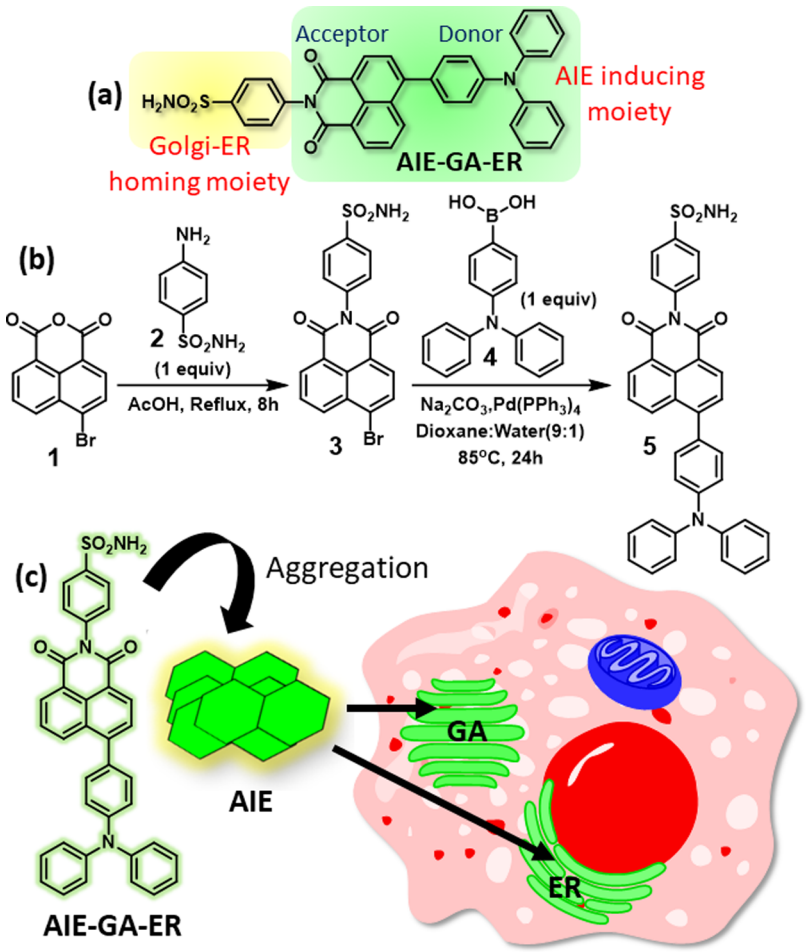

Figure 1. (a) Structure of the AIE-GA-ER molecule. (b) Synthetic scheme of the AIE-GA-ER. (c) Schematic representation of the AIE-GA-ER to illuminate Golgi apparatus and ER inside the cells.

apparatus and ER remains limited, indicating that this area is still in its nascent stages.[49−55]

To address this, herein, we have designed and synthesized a small molecule AIEgen (AIE-GA-ER) comprising (a) phenylsulfonamide as Golgi-ER homing moiety, (b) 1,8-naphthalimide-triphenylamine to induce aggregation-induced emission property, and (c) donor (triphenylamine)-acceptor (naphthalimide) moiety for triggering intramolecular charge transfer (ICT) by a concise strategy (Figure 1a,b). Interestingly, AIE-GA-ER demonstrated remarkable "on-off-on" AIE properties in THF/water and "off-on" AIE in DMSO/water binary solvent systems. Dynamic light scattering (DLS) and scanning electron microscopy (SEM) revealed that AIE-GA-ER exhibited self-assembled structures in pure THF and 80% water/THF mixture validating the luminescence induced by aggregated states. The molecular dynamics simulation (MD) and density functional theory (DFT) calculations showed that the interplay between intramolecular charge transfer (ICT) stabilization and aggregation controlled the emissive behavior of the AIE-GA-ER in THF, DMSO, and water as well in the binary solvent mixtures. Fluorescence confocal microscopy confirmed that AIE-GA-ER successfully homed into and illuminated the Golgi apparatus of colon cancer cells (HCT-116) within 15−30 min as well as cervical cancer cells (HeLa) and noncancerous human retinal epithelial pigment cells (RPE-1) within 3h without toxicity (Figure 1c). Interestingly, although AIE-GA-ER marginally localized into the other organelles like mitochondria and lysosomes, it localized into the endoplasmic reticulum (ER) efficiently within 15−30 min, indicating a cross-talk between Golgi and ER related to the protein and lipid secretion between them. We anticipate this novel "on-off-on" AIE-GA-ER probe can be a powerful tool to understand the subcellular hydrophobic−hydrophilic microenvironment inside specific organelles, as well as the cross-talk between Golgi apparatus and ER in cancer cells for therapeutic outcome.

RESULTS AND DISCUSSION

We have designed the AIE-GA-ER by introducing (a) phenylsulfonamide moiety for Golgi homing due to its ability to bind with the Cox-2 enzyme localized into the Golgi apparatus[29,31−33] and (b) 1,8-napthalimide-triphenylamine moiety for its ability to activate aggregation-induced emission (AIE) (Figure 1a). We first coupled 4-bromo-1,8-napthalic anhydride (1) with 4-aminobenzene sulphonamide (2) in the presence of acetic acid in refluxing condition to afford 4-bromo-1,8-napthalic-benzenesulfonamide (3). Compound 3 was then reacted with 4-(diphenylamino) phenylboronic acid (4) in Suzuki coupling condition using $Pd(PPh_3)_4$ as a catalyst to obtain AIE-GA-ER (5) in 80% yield (Figure 1b). Compound 3 and compound 5 were characterized by ^1H, ^{13}C NMR, and HR-MS spectra (Figures S1−S6).

To evaluate the photophysical properties, we assessed the UV−vis spectroscopy of the AIE-GA-ER in different solvents.

https://doi.org/10.1021/acsabm.4c01722
ACS Appl. Bio Mater. XXXX, XXX, XXX−XXX

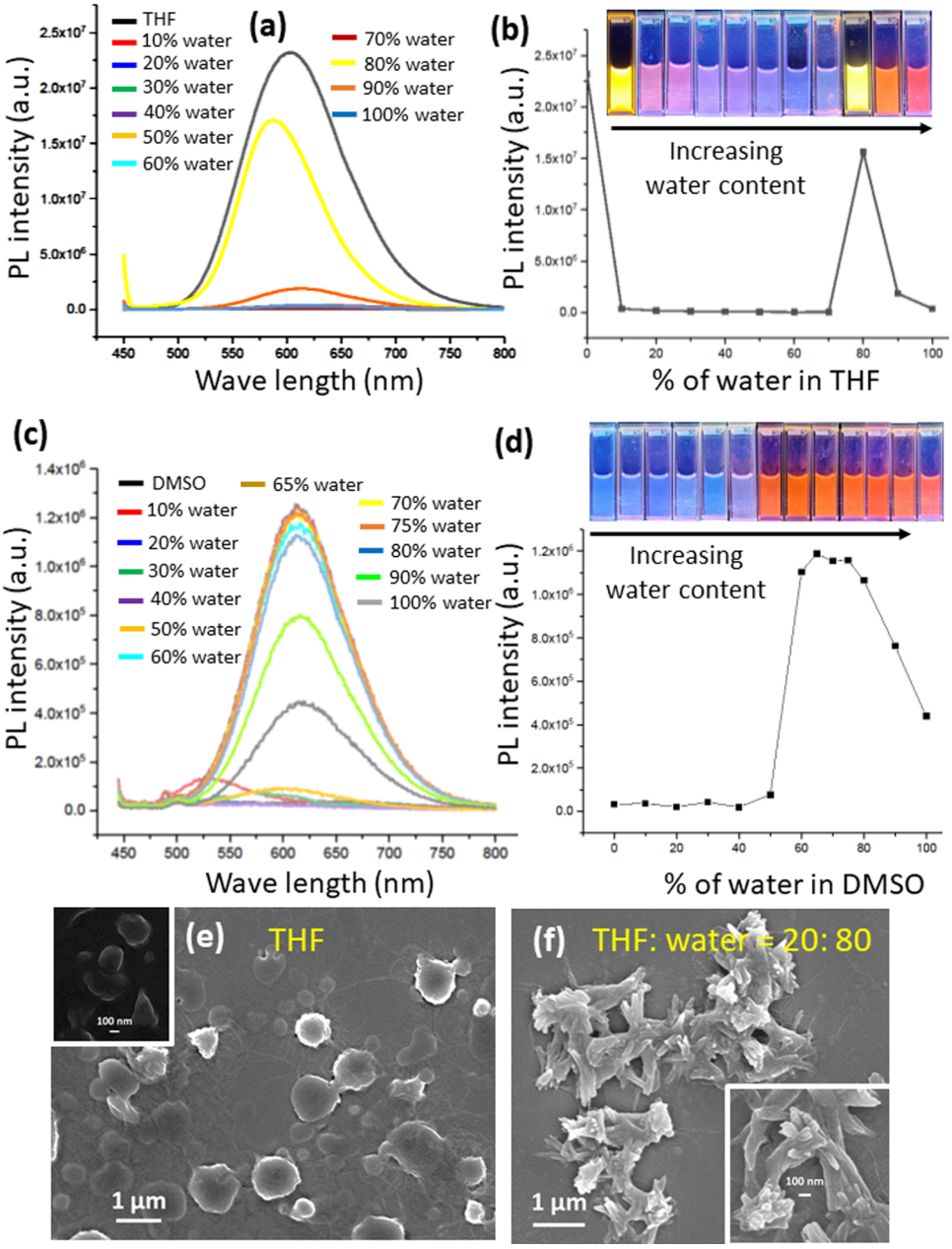

Figure 2. (a) Change in fluorescence emission spectra of AIE-GA-ER (20 μM) in different THF/water ratios. The molecule was excited at 439 nm. (b) Fluorescence emission intensity versus water fraction graph of the AIE-GA-ER. Inset: Cuvette images of AIE-GA-ER in different THF/water mixtures. (c) Change in the fluorescence emission spectra of AIE-GA-ER (20 μM) in different DMSO/Water ratios. (d) Fluorescence emission intensity versus water fraction graph of AIE-GA-ER. Inset: Cuvette images of AIE-GA-ER in different DMSO/water mixtures. The molecule was excited at 439 nm. (e, f) SEM images of AIE-GA-ER in THF and 80% water in the THF mixture.

AIE-GA-ER showed absorbance peaks at λ_{max} = 306-310 and 421−450 nm in THF, methanol, DMSO, acetonitrile, and water (Figure S7). It is noted that the λ_{max} is red-shifted, became a little broad with reduced absorbance compared to the other organic solvents, and indicated a potential aggregation behavior in water. We further evaluated the fluorescence emission of AIE-GA-ER in THF which interestingly exhibited a high fluorescence emission at λ_{em} = 604 nm (Figure 2a). However, the fluorescence emission was dramatically quenched when water was added into the THF solution from 10% water/THF until the 70% water/THF mixture (Figure 2a,b). Remarkably, the fluorescence emission of AIE-GA-ER was increased sharply at 80% water/THF mixture. This fluorescence emission of AIE-GA-ER in THF/water binary solvent confirmed the "on-off-on" emissive behavior which was in accordance with the "on-off-on" AIEgen nanoparticle for time-resolved fluorescence imaging of lipid droplets in cancer cells.[56] We further evaluated the fluorescence lifetime of AIE-GA-ER in THF and 80% water in THF. AIE-GA-ER showed a 3.81 ns fluorescence lifetime in THF (Figure S8). On the contrary, in 80% water in THF, AIE-GA-ER showed much less fluorescence lifetimes of 0.13 and 1.38 ns. Moreover, AIE-GA-ER showed a high quantum yield of 29% in THF.

We further evaluated the fluorescence emission of AIE-GA-ER in a DMSO/water system. AIE-GA-ER exhibited negligible

https://doi.org/10.1021/acsabm.4c01722
ACS Appl. Bio Mater. XXXX, XXX, XXX−XXX

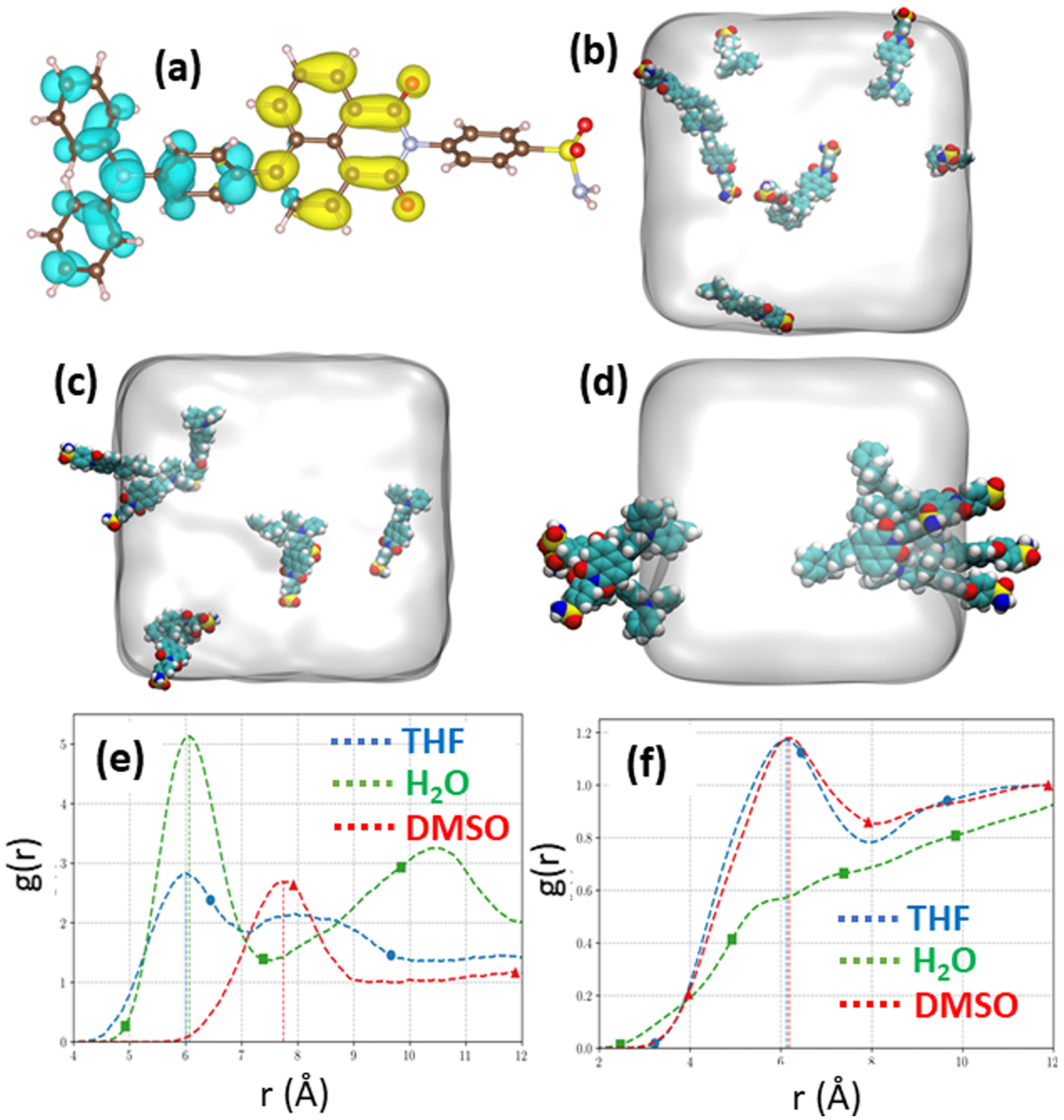

Figure 3. (a) Density difference plot illustrating regions of increased (yellow) and decreased (blue) electron density during the S_1 to S_0 transition, highlighting the charge transfer direction within the AIE-GA-ER. (b−d) Aggregation pattern of AIE-GA-ER in DMSO, THF and water, respectively. (e) Radial distribution functions (RDF) of AIE-GA-ER between nitrogen (N) atoms of the triphenylamine moiety in different solvents (f) RDF between the center of mass of the solute (AIE-Golgi) and the center of mass of the solvent molecules in different solvents.

fluorescence emission in DMSO until 50% water/DMSO mixture (Figure 2c). However, the fluorescence emission remarkably increased at the 60% water/DMSO mixture at λ_{em} = 628 nm (Figure 2c,d). Interestingly, in 100% water, the emission of AIE-GA-ER was reduced, however, not quenched entirely, giving us the opportunity to image the Golgi apparatus inside the cells. The quantum yield of AIE-GA-ER was calculated to be 3.7% in water. We validated the aggregation phenomena of AIE-GA-ER in THF and 80% water/THF mixture by dynamic light scattering (DLS). The DLS histogram showed sharp and narrow peaks of AIE-GA-ER in THF with hydrodynamic diameter = 2314 nm (Figure S9a). On the contrary, AIE-GA-ER showed a broad histogram indicating polydispersity in 80% water/THF with a much lower hydrodynamic diameter of 495.6 nm (Figure S9b). Similarly, the DLS of AIE-GA-ER in pure water showed a 227.8 nm hydrodynamic diameter with two distributions (Figure S9c). The DLS clearly indicated the formation of different-sized aggregates of AIE-GA-ER in both pure THF, water, and an 80% water/THF mixture. To further confirm the aggregation of AIE-GA-ER in THF, water, and 80% water/THF mixture, we visualized the aggregation formation by scanning electron microscopy (SEM) and atomic force microscopy (AFM). From the SEM images, we observed that AIE-GA-ER formed spherical self-assembled aggregates in THF (Figure 2e). However, in the 80% water/THF mixture, AIE-GA-ER changed its morphology into 2D-sheet-like self-assembled aggregates (Figure 2f). Interestingly, AIE-GA-ER showed a fused spherical morphology in water different from the morphology observed in THF and 80% water in THF (Figure S10). From the AFM images, we also visualized that AIE-GA-ER self-assembled into spherical nanoparticles in THF but showed 2D sheet-like structures in 80% water/THF and fused spherical morphology in water (Figure S11). Moreover,

https://doi.org/10.1021/acsabm.4c01722
ACS Appl. Bio Mater. XXXX, XXX, XXX−XXX

we confirmed the aggregate formation in THF, water, and 80% water in THF by the Tyndall effect which clearly showed that AIE-GA-ER aggregated weakly in THF, but effectively in 80% water in THF and water (Figure S12). Furthermore, we also evaluated the aggregation of AIE-GA-ER in the DMSO/water mixture by DLS. In DMSO, AIE-GA-ER showed negligible particle distribution with a very low hydrodynamic diameter of 4.8 nm (Figure S13a). On the other hand, in 60% water in DMSO, AIE-GA-ER showed a broad distribution of particles with a hydrodynamic diameter of 115.4 nm (Figure S13b). This DLS data indicated that AIE-GA-ER exhibited marginal aggregation in DMSO but aggregated in 60% water in the DMSO solvent system. We further checked the aggregation of AIE-GA-ER in DMSO and 60% water in DMSO by the Tyndall effect, which clearly showed that AIE-GA-ER aggregated in 60% water in DMSO solvent system, but not in DMSO (Figure S14). These DLS, SEM, AFM, and Tyndall effects clearly confirmed that AIE-GA-ER self-assembled into aggregates in THF, water, 80% water in THF, and 60% water in DMSO, validating the AIE property.

We substantiated the interesting photophysical property of AIE-GA-ER by quantum mechanical calculations to determine whether the charge transfer within the molecule is long-range or short-range. The resulting density difference plot for the S_1 and S_0 transition state displayed two distinct color patterns: (a) the blue regions are concentrated on the *N*,*N*,*N*-triphenyl amine moiety, indicating its role as the electron donor and (b) the yellow regions are predominantly located on the carbonyl-containing moieties in the naphthalimide, signifying its role as the electron acceptor (Figure 3a). Hence, the overall charge transfer is directed from the *N*,*N*,*N*-triphenylamine to the 1,8-naphthalimide moiety, suggesting a long-range charge transfer (LRCT) mechanism. On the contrary, short-range charge transfer (SRCT) would have shown yellow and blue lobes on the alternative atoms. To further quantify the nature of charge transfer, we calculated the charge transfer number (Q_{CT}) and the overlap integral ($S_{\pm}$) between the donor and acceptor regions. The Q_{CT} value ranges from 0 to 1, where values closer to 0 indicate SRCT and values closer to 1 suggest LRCT. Similarly, the overlap integral provides insight into the extent of charge transfer overlap; a value near 0 supports LRCT, while a value close to 1 indicates SRCT. In our analysis, the calculated Q_{CT} for AIE-GA-ER was found to be 0.9, while the overlap integral was found to be 0.13, indicating that AIE-GA-ER exhibited long-range charge transfer. This quantitative assessment aligns with our qualitative observations, providing a comprehensive understanding of the charge transfer behavior within the molecule.[57−59]

To validate the intramolecular charge transfer (ICT), we evaluated the fluorescence emission of AIE-GA-ER in different polar (water, DMSO, methanol, acetonitrile, and DMF) and nonpolar solvents (chloroform, dichloromethane, toluene, THF, and 1,4-dioxane). The solvent-dependent fluorescence studies of the AIE-GA-ER revealed a clear distinction in emission intensity and wavelength maxima between polar and nonpolar solvents, highlighting the molecule's intramolecular charge transfer (ICT) characteristics. In polar solvents, a significant reduction in fluorescence intensity was observed, which can be attributed to the stabilization of the ICT excited state by polar environments (Figure S15a). This stabilization increases the nonradiative decay pathways, leading to fluorescence quenching. In contrast, nonpolar solvents restricted the stabilization of the ICT state, reducing nonradiative decay and resulting in enhanced fluorescence intensity. Among nonpolar solvents, the trend in the emission wavelength maxima (dichloromethane > chloroform > THF > 1,4-dioxane > toluene) suggests that the emission is sensitive to both solvent polarity and polarizability (Figure S15b). Dichloromethane and chloroform, being more polarizable nonpolar solvents, stabilized the ICT state more effectively, resulting in a red-shifted emission. On the other hand, solvents like toluene and 1,4-dioxane, with lower polarity and polarizability, exhibited relatively blue-shifted emissions. This trend also indicated the presence of specific solvent-molecule interactions, such as dipole−dipole interactions and hydrogen bonding, which further influenced the stabilization of the ICT state. For instance, due to their higher dipole moments, dichloromethane and chloroform interacted more strongly with the ICT state, leading to greater stabilization and red-shifted emission. Overall, the observed solvent-dependent emission behavior provided compelling evidence of the ICT nature of the AIE-GA-ER molecule. These findings not only validated the claim of ICT but also offered valuable insights into the photophysical properties of the molecule under different solvent environments.

The photophysical parameters, e.g., emission wavelength (λ) in nm and energy of the first singlet state (ES_1) in eV of AIE-GA-ER in THF and DMSO were calculated by density functional theory (DFT) and are summarized in Table S1. Two key factors influence the emission properties of the molecule in solution: charge transfer (CT) stabilization and aggregation-induced emission (AIE). CT stabilization occurs when there is a "like-dissolves-like" interaction between the solute and solvent, such as a polar solute in a polar solvent or a nonpolar solute in a nonpolar solvent. However, if over-stabilization occurs, solute−solvent interactions become highly favored, decreasing emission intensity. From Table S1, it is evident that as we change the solvent from THF to DMSO, AIE-GA-ER experiences a bathochromic shift of approximately 10 nm, indicating a decrease in the energy gap between the first singlet state (S_1) and the ground state (S_0). This suggests that DMSO effectively stabilizes the S_1 state, leading to the over stabilization of the CT state. The shift in wavelength is not very pronounced, which could be attributed to using an implicit solvation model, thereby reducing the observed effect.

We further investigated the aggregation behavior of AIE-GA-ER in different environments by molecular dynamics (MD) simulations using a system consisting of 8 organic molecules and 2000 solvent molecules and evaluated the morphologies in different solvents. In DMSO (Figure 3b), the AIE-GA-ER did not show any aggregation, whereas in THF (Figure 3c) and water (Figure 3d), the AIE-GA-ER was inclined to aggregate, as evident from their closer spatial arrangement. To quantitatively analyze the aggregation behavior, we further calculated the radial distribution functions (RDFs). The RDFs shown in Figure 3e were generated using the nitrogen (N) atom of the triphenylamine moiety as a reference, with respect to the N atoms of neighboring molecules. This RDF provided insights into the spatial distribution and proximity of the molecules. The *y*-axis represents $g(r)$, proportional to the probability of finding a molecule at a specific distance from another molecule, indicated on the *x*-axis. The RDFs for THF and water exhibited peaks at shorter distances, specifically around 6 Å, indicating that the N atoms of triphenylamine were closer in these solvents than DMSO, where the distance was found to be approximately 7.8 Å. This finding suggested

https://doi.org/10.1021/acsabm.4c01722
ACS Appl. Bio Mater. XXXX, XXX, XXX−XXX

that AIE-GA-ER tends to aggregate in THF and water, while in DMSO, no significant aggregation was observed.

We calculated the distribution of the center of mass of AIE-GA-ER relative to the center of mass of the solvent molecules, which provided insights into the spatial arrangement of solvent molecules around the solute. The RDFs for DMSO and THF exhibited peaks at shorter distances, suggesting favorable solute−solvent interactions (Figure 3f). This behavior can be attributed to the substantial hydrophobic regions in the AIE-GA-ER, such as the nonpolar benzene rings, which interact favorably with the methyl groups of DMSO and the organic five-membered ring moieties of THF. Conversely, the first peak in the RDF for water was observed at a significantly larger distance, indicating weaker solute−solvent interactions. This reduced interaction was likely due to the absence of methyl or other hydrophobic moieties in water, leading to a limited interaction with the organic solute. Consequently, the AIE-GA-ER aggregated, thereby restricting the space available for water molecules, which resulted in the RDF peak appearing at a greater distance. In a polar solvent such as DMSO, the solute−solvent interactions are highly favored, stabilizing the CT state effectively. This stabilization reduced the likelihood of aggregation, as the solute remained well-dispersed due to the strong solvation effect. In contrast, in THF and water, the solvation of the ICT state was less efficient. In water, hydrophobic interactions triggered aggregation, as the hydrophobic regions of AIE-GA-ER minimized contact with the polar solvent. Similarly, in THF, weaker solvation of the polar groups in AIE-GA-ER leads to increased solute−solute interactions and, hence, aggregation.

These MD and DFT calculations revealed that the emission behavior of AIE-GA-ER across different solvents was influenced by the interplay between intramolecular charge transfer (ICT) stabilization and aggregation. In pure DMSO, the emission was suppressed due to overstabilization of the ICT state and the absence of aggregation, resulting in minimal emission. In THF, the solvent provided moderate stabilization of the ICT state without leading to overstabilization, allowing aggregation-induced emission (AIE) to dominate and yield the highest emission intensity. Upon the addition of water, aggregation persisted and promoted emission; however, the emission intensity was reduced compared to pure THF, as water also stabilized the ICT state to some extent. Thus, the combination of ICT state stabilization and aggregation behavior determined the overall emission properties, with THF showing the maximum emission, followed by the water mixture and DMSO exhibiting minimal emission leading to a unique "on-off-on" AIE property.

To be effective in bioimaging, the AIEgen should ideally be nontoxic. Hence, to evaluate the toxicity profile, we treated HCT-116 colon cancer cells as well as noncancerous RPE-1 human retinal epithelial pigment cells with AIE-GA-ER in a dose-dependent manner for 3h and the cell viability was evaluated by MTT assay. The MTT assay exhibited no toxicity of AIE-GA-ER in HCT-116 and RPE-1 cells at 3h which will be an ideal time for bioimaging of the Golgi apparatus and ER (Figure S16).

Before checking the subcellular homing, we assessed the cellular uptake of AIE-GA-ER in HCT-116 cells. We treated HCT-116 cells with AIE-GA-ER in a time-dependent manner for 15 min, 30 min, and 1 h and visualized the cells under confocal microscopy. The confocal images clearly showed that at 15 min, a small amount of AIE-GA-ER was taken up by HCT-116 cells, leading to weak green fluorescence signals (Figure S17a). However, at 30 min and 1 h, the green fluorescence intensity increased by 2.7 and 5.5-fold, respectively, compared to the fluorescence intensity observed at 15 min (Figure S17b). This confocal microscopy confirmed that AIE-GA-ER was taken up by HCT-116 cells in a time-dependent manner over 1 h.

To evaluate the effectiveness of AIE-GA-ER in visualizing Golgi apparatus in cancer cells, we incubated HCT-116 colon cancer cells with AIE-GA-ER for 15 min, 30 min, 1 h, and 3 h. The Golgi apparatus was stained with commercially available GolgiTracker Red dye and the cells were visualized by confocal microscopy. The confocal images exhibited that green fluorescence AIE-GA-ER localized into the red fluorescent Golgi apparatus efficiently in a time-dependent manner within 15 min yielding merged yellow signals in HCT-116 cells with Pearson's correlation coefficients (PCC) of 0.77, 0.88, 0.80, and 0.84 respectively (Figures 4 and S18) along with Mander's

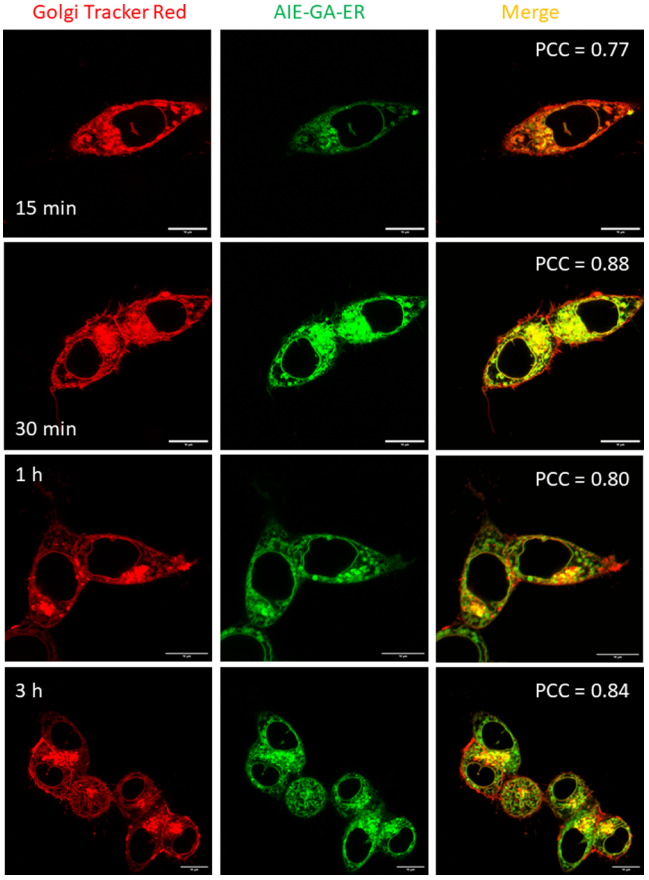

Figure 4. Confocal laser scanning microscopy images of HCT-116 cells incubated with AIE-GA-ER (green) for 15 min, 30 min, 1 h, and 3 h, followed by staining the Golgi apparatus by GolgiTracker Red dye. Scale bar = 10 μm.

coefficients of 0.84, 0.96, 0.95, and 0.97 respectively. We also checked the homing of AIE-GA-ER into the HeLa cervical cancer cells at a 3 h time point by confocal microscopy, which showed that AIE-GA-ER also localized into the Golgi apparatus of HeLa cells efficiently within 3 h with PCC and Mander's coefficient = 0.77 and 0.99, respectively (Figure S19a). We further evaluated the usefulness of AIE-GA-ER to illuminate the Golgi apparatus in noncancerous human epithelial retinal pigment (RPE-1) cells. We incubated RPE-1

https://doi.org/10.1021/acsabm.4c01722
ACS Appl. Bio Mater. XXXX, XXX, XXX−XXX

cells with AIE-GA-ER for 3 h, costained the Golgi apparatus with GolgiTracker Red, and visualized the cells under confocal microscopy. The confocal images revealed that AIE-GA-ER efficiently homed into the Golgi apparatus of RPE-1 cells within 3 h with PCC = 0.78 and Mander's coefficient = 0.98 (Figure S19b).

We further evaluated the homing of the AIE-GA-ER in the ER in HCT-116 cells. We incubated HCT-116 cells with AIE-GA-ER at 15 min, 30 min, 1 h, and 3 h time points followed by staining the ER with ER Tracker Red dye, and the live cells were visualized by confocal microscopy. Interestingly, the confocal microscopy images revealed that AIE-GA-ER also homed into the ER efficiently leading to the generation of merged yellow fluorescence signals with PCC = 0.8, 0.89, 0.88, and 0.84 for 15 min, 30 min, 1 h, and 3 h, respectively, having Mander's coefficients of 0.85, 0.94, 0.94, and 0.96 (Figures 5 and S20). We rationalize that this simultaneous homing of AIE-GA-ER into the Golgi apparatus and ER is due to the secretion-mediated cross-talk between the Golgi apparatus and ER in cancer cells.[24,60−62]

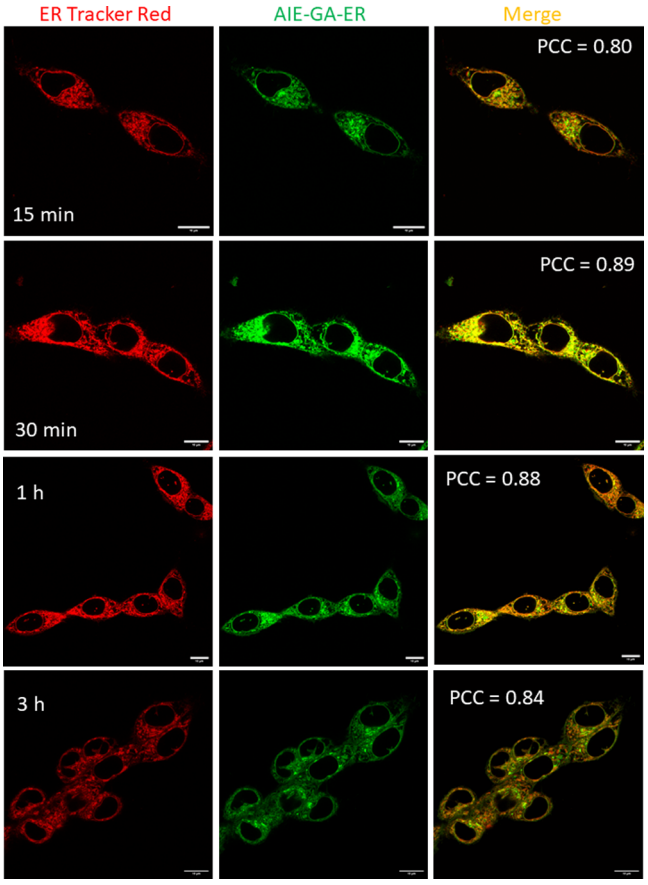

Figure 5. Confocal laser scanning microscopy images of the HCT-116 cells incubated with AIE-GA-ER for 3 h, followed by staining the endoplasmic reticulum (ER) by ER Tracker Red dye. Scale bar = 10 μm.

Furthermore, we assessed the homing of AIE-GA-ER in other organelles such as mitochondria and lysosomes in HCT-116 cells. We treated HCT-116 cells with AIE-GA-ER for 3 h and stained the mitochondria and lysosomes with MitoTracker Red and LysoTracker Red dyes, followed by visualizing the cells under confocal microscopy. The confocal images demonstrated that AIE-GA-ER marginally homed into the mitochondria and lysosomes with lower PCC = 0.62 and 0.42, respectively (Figure S21). Although from this confocal imaging quantification, AIE-GA-ER seemed homing into the mitochondria with moderate PCC = 0.62, we could not visualize typical filamentous mitochondrial morphology by AIE-GA-ER. We reasoned that AIE-GA-ER localized into the ER near the mitochondria-ER membrane which could only be spatially visualized by super-resolution time-resolved fluorescence microscopy. These confocal images evidently confirmed that AIE-GA-ER can simultaneously home into the Golgi apparatus and ER of HCT-116, HeLa, and RPE-1 cells proficiently within 15−30 min with marginal localization into the mitochondria and lysosomes.

CONCLUSIONS

In conclusion, we have designed and synthesized a novel 1,8-napthalimide-triphenylamine-sulfonamide-based small molecule (AIE-GA-ER) that exhibited remarkable "on-off-on" emissive behavior in a THF/water mixture and 'off-on" emissive property in a DMSO/water mixture through aggregation-induced emission (AIE). The self-assembled aggregation of AIE-GA-ER was confirmed by DLS, SEM, and AFM images. MD and DFT studies revealed the underlying mechanism of this unique AIE behavior of the AIE-GA-ER as the interplay between intramolecular long-range charge transfer (LRCT) stabilization and aggregation in THF, DMSO, and water. The AIE-GA-ER remarkably illuminated the Golgi apparatus and ER within 15−30 min in the HCT-116 colon cancer cells as well as in the cervical cancer cells (HeLa) and noncancerous cells (RPE-1) without toxicity. This novel AIE-GA-ER probe has the potential to be used as a tool to understand the subcellular hydrophobic-hydrophilic microenvironment inside different organelles and the cross-talk between the Golgi apparatus and ER in cancer cells.

ASSOCIATED CONTENT

Supporting Information

The Supporting Information is available free of charge at https://pubs.acs.org/doi/10.1021/acsabm.4c01722.

NMR spectra, HR-MS, UV-vis spectra, fluorescence spectra, DLS, FESEM, AFM, MTT assay, confocal microscopy (PDF)

AUTHOR INFORMATION

Corresponding Authors

Anirban Mondal − *Department of Chemistry, Indian Institute of Technology Gandhinagar, Gandhinagar, Gujarat 382355, India;* orcid.org/0000-0003-3029-8840; Email: amondal@iitgn.ac.in

Sudipta Basu − *Department of Chemistry, Indian Institute of Technology Gandhinagar, Gandhinagar, Gujarat 382355, India;* orcid.org/0000-0002-0433-8899; Email: sudipta.basu@iitgn.ac.in

Authors

Phanindra Kumar − *Department of Chemistry, Indian Institute of Technology Gandhinagar, Gandhinagar, Gujarat 382355, India*

Tripti Mishra − *Department of Chemistry, Indian Institute of Technology Gandhinagar, Gandhinagar, Gujarat 382355, India*

https://doi.org/10.1021/acsabm.4c01722
ACS Appl. Bio Mater. XXXX, XXX, XXX−XXX

Sanyam − *Department of Chemistry, Indian Institute of Technology Gandhinagar, Gandhinagar, Gujarat 382355, India;* orcid.org/0000-0001-7410-8207

Complete contact information is available at: https://pubs.acs.org/10.1021/acsabm.4c01722

Author Contributions

‡P.K. and T.M. contributed equally to this work.

Notes

The authors declare no competing financial interest.

■ ACKNOWLEDGMENTS

S.B. sincerely thanks IIT Gandhinagar, Gujarat Council on Science and Technology (GUJCOST/STI/R&D/2020-21/1302), and the Science and Engineering Research Board (CRG/2020/001127) for funding. P.K. acknowledges CSIR-UGC-JRF for a doctoral fellowship. T.M. thanks IIT Gandhinagar for the doctoral fellowship. Sanyam thanks CSIR for the fellowship. Sanyam and A.M, thank IITs Gandhinagar for its research facilities.

■ REFERENCES

(1) Tang, D.; Wang, Y. Cell cycle regulation of Golgi membrane dynamics. *Trends Cell Biol.* **2013**, *23*, 296−304.
(2) Shorter, J.; Warren, G. Golgi architecture and inheritance. *Annu. Rev. Cell Dev. Biol.* **2002**, *18*, 379−420.
(3) Wang, Y.; Seemann, J. Golgi biogenesis. *Cold Spring Harb Perspect Biol.* **2011**, *3*, No. a005330.
(4) Farquhar, M. G.; Palad, G. E. The Golgi apparatus: 100 years of progress and controversy. *Trends Cell Biol.* **1998**, *8*, 2−10.
(5) Marsh, B. J.; Howell, K. E. The mammalian Golgi—complex debates. *Nat. Rev. Mol. Cell Biol.* **2002**, *3*, 789−795.
(6) Liu, J.; Huang, Y.; Li, T.; Jiang, Z.; Zeng, L.; Hu, Z. The role of the Golgi apparatus in disease. *Int. J. Mol. Med.* **2021**, *47*, 38.
(7) Anelli, T.; Sitia, R. Protein quality control in the early secretory pathway. *EMBO J.* **2008**, *27*, 315−327.
(8) Pizzo, P.; Pozzan, T. Mitochondria−endoplasmic reticulum choreography: structure and signaling dynamics. *Trends Cell Biol.* **2007**, *17*, 511−517.
(9) Ma, Y.; Hendershot, L. M. ER chaperone functions during normal and stress conditions. *J. Chem. Neuroanat.* **2004**, *28*, 51−65.
(10) Kim, I.; Xu, W.; Reed, J. C. Cell death and endoplasmic reticulum stress: disease relevance and therapeutic opportunities. *Nat. Rev. Drug Discovery* **2008**, *7*, 1013−1030.
(11) Buschman, M. D.; Rahajeng, J.; Field, S. J. GOLPH3 Links the Golgi, DNA Damage, and Cancer. *Cancer. Res.* **2015**, *75*, 624−627.
(12) Song, J. W.; Zhu, J.; Wu, X. X.; Tu, T.; Huang, J. Q.; Chen, G. Z.; Liang, L. Y.; Zhou, C. H.; Xu, X.; Gong, L. Y. GOLPH3/CKAP4 promotes metastasis and tumorigenicity by enhancing the secretion of exosomal WNT3A in non-small-cell lung cancer. *Cell Death Dis.* **2021**, *12*, 976.
(13) Bajaj, R.; Warner, A. N.; Fradette, J. F.; Gibbons, D. L. Dance of the Golgi: understanding Golgi dynamics in cancer metastasis. *Cells.* **2022**, *11*, 1484.
(14) Bajaj, R.; Kundu, S. T.; Grzeskowiak, C. L.; Fradette, J. J.; Scott, K. L.; Creighton, C. J.; Gibbons, D. L. IMPAD1 and KDELR2 drive invasion and metastasis by enhancing Golgi-mediated secretion. *Oncogene.* **2020**, *39*, 5979−5994.
(15) Gupta, R.; Malvi, P.; Parajuli, K. R.; Janostiak, R.; Bugide, S.; Cai, G.; Zhu, L. J.; Green, M. R.; Wajapeyee, N. KLF7 promotes pancreatic cancer growth and metastasis by up-regulating ISG expression and maintaining Golgi complex integrity. *Proc. Natl. Acad. Sci. U. S. A.* **2020**, *117*, 12341−12351.
(16) Raina, K.; Noblin, D. J.; Serebrenik, Y. V.; Adams, A.; Zhao, C.; Crews, C. M. Targeted protein destabilization reveals an estrogen-mediated ER stress response. *Nat. Chem. Biol.* **2014**, *10*, 957−962.
(17) Maly, D. J.; Papa, F. R. Druggable sensors of the unfolded protein response. *Nat. Chem. Biol.* **2014**, *10*, 892−901.
(18) Wang, M.; Kaufman, R. J. Protein misfolding in the endoplasmic reticulum as a conduit to human disease. *Nature.* **2016**, *529*, 326−335.
(19) Smith, M. H.; Ploegh, H. L.; Weissman, J. S. Road to ruin: targeting proteins for degradation in the endoplasmic reticulum. *Science* **2011**, *334*, 1086−1090.
(20) Chen, X.; Cubillos-Ruiz, J. R. Endoplasmic reticulum stress signals in the tumour and its microenvironment. *Nat. Rev. Cancer.* **2021**, *21*, 71−88.
(21) Marciniak, S. J.; Chambers, J. E.; Ron, D. Pharmacological targeting of endoplasmic reticulum stress in disease. *Nat. Rev. Drug Discovery* **2022**, *21*, 115−140.
(22) Zhang, Y.; Wu, Y.; Zhang, M.; Li, Z.; Liu, B.; Liu, H.; Hao, J.; Li, X. Synergistic mechanism between the endoplasmic reticulum and mitochondria and their crosstalk with other organelles. *Cell Death Dis.* **2023**, *9*, 51.
(23) Zhang, H.; Rui, M.; Ma, Z.; Gong, S.; Zhang, S.; Zhou, Q.; Gan, C.; Gong, W.; Wang, S. Golgi-to-ER retrograde transport prevents premature differentiation of Drosophila type II neuroblasts via Notch-signal-sending daughter cells. *iScience* **2024**, *27*, No. 108545.
(24) Wlodkowic, D.; Skommer, J.; McGuinness, D.; Hillier, C.; Darzynkiewicz, Z. ER−Golgi network—A future target for anti-cancer therapy. *Leuk. Res.* **2009**, *33*, 1440−1447.
(25) Zhang, H.; Fan, J.; Wang, J.; Zhang, S.; Dou, B.; Peng, X. An off−on Cox-2-specific fluorescent probe: Targeting the golgi apparatus of cancer cells. *J. Am. Chem. Soc.* **2013**, *135*, 11663−11669.
(26) Hu, X.; Hai, Z.; Wu, C.; Zhan, W.; Liang, G. A golgi-targeting and dual-color "turn-on" probe for spatially precise imaging of furin. *Anal. Chem.* **2021**, *93*, 1636−1642.
(27) Fortibui, M. M.; Lim, W.; Lee, S.; Park, S.; Kim, J. A golgi apparatus-targeting, naphthalimide-based fluorescent molecular probe for the selective sensing of formaldehyde. *Molecules.* **2021**, *26*, 4980.
(28) Hirayama, T.; Inden, M.; Tsuboi, H.; Niwa, M.; Uchida, Y.; Naka, Y.; Hozumi, I.; Nagasawa, H. A Golgi-targeting fluorescent probe for labile Fe (ii) to reveal an abnormal cellular iron distribution induced by dysfunction of VPS35. *Chem. Sci.* **2019**, *10*, 1514−1521.
(29) Wang, H.; He, Z.; Yang, Y.; Zhang, J.; Zhang, W.; Zhang, W.; Li, P.; Tang, B. Ratiometric fluorescence imaging of Golgi H_2O_2 reveals a correlation between Golgi oxidative stress and hypertension. *Chem. Sci.* **2019**, *10*, 10876−10880.
(30) Sawada, S.; Yoshikawa, M.; Tsutsui, K.; Miyazaki, T.; Kano, K.; Mishiro-Sato, E.; Tsukiji, S. Palmitoylation-dependent small-molecule fluorescent probes for live-cell Golgi imaging. *ACS Chem. Biol.* **2023**, *18*, 1047−1053.
(31) Yuan, M.; Hu, J.; Chen, W. H. Synthesis of a Golgi-targeting fluorescent probe for the selective detection of chloride anions. *Org. Biomol. Chem.* **2023**, *21*, 5732−5736.
(32) Xu, S.; Yan, K. C.; Xu, Z. H.; Wang, Y.; James, T. D. Fluorescent probes for targeting the Golgi apparatus: design strategies and applications. *Chem. Soc. Rev.* **2024**, *53*, 7590−7631.
(33) Li, S.; Yang, K.; Zeng, J.; Ding, Y.; Cheng, D.; He, L. Golgi-targeting fluorescent probe for monitoring CO-releasing molecule-3 in vitro and in vivo. *ACS Omega.* **2022**, *7*, 9929−9935.
(34) Wang, H.; Zhang, X.; Xiu, T.; Wang, H.; Li, P.; Tang, B. Fluorescence probes for sensing and imaging within Golgi apparatus. *Coord. Chem. Rev.* **2024**, *502*, No. 215618.
(35) Mei, J.; Leung, N. L.; Kwok, R. T.; Lam, J. W.; Tang, B. Z. Aggregation-induced emission: together we shine, united we soar! *Chem. Rev.* **2015**, *115*, 11718−11940.
(36) Liu, B.; Zhang, R. Aggregation induced emission: concluding remarks. *Faraday Discussions.* **2017**, *196*, 461−472.
(37) Jiang, X.; Gao, H.; Zhang, X.; Pang, J.; Li, Y.; Li, K.; Wu, Y.; Li, S.; Zhu, J.; Wei, Y.; Jiang, L. Highly-sensitive optical organic vapor sensor through polymeric swelling induced variation of fluorescent intensity. *Nat. Commun.* **2018**, *9*, 3799.

(38) Chen, Y.; Min, X.; Zhang, X.; Zhang, F.; Lu, S.; Xu, L. P.; Lou, X.; Xia, F.; Zhang, X.; Wang, S. AIE-based superwettable microchips for evaporation and aggregation induced fluorescence enhancement biosensing. *Biosensors and Bioelectronics.* **2018**, *111*, 124−130.
(39) Qi, J.; Chen, C.; Ding, D.; Tang, B. Z. Aggregation-induced emission luminogens: union is strength, gathering illuminates healthcare. *Adv. Healthc. Mater.* **2018**, *7*, No. 1800477.
(40) Zhu, C.; Kwok, R. T.; Lam, J. W.; Tang, B. Z. Aggregation-induced emission: a trailblazing journey to the field of biomedicine. *ACS Appl. Bio Mater.* **2018**, *1*, 1768−1786.
(41) Hu, F.; Liu, B. Organelle-specific bioprobes based on fluorogens with aggregation-induced emission (AIE) characteristics. *Org. Biomol. Chem.* **2016**, *14*, 9931−9944.
(42) Qian, J.; Tang, B. Z. AIE luminogens for bioimaging and theranostics: from organelles to animals. *Chem.* **2017**, *3*, 56−91.
(43) Niu, G.; Zhang, R.; Kwong, J. P. C.; Lam, J. W.; Chen, C.; Wang, J.; Chen, Y.; Feng, X.; Kwok, R. T.; Sung, H. H. Y.; Williams, I. D.; Elsegood, M. R. J.; Qu, J.; Ma, C.; Wong, K. S.; Yu, X.; Tang, B. Z. Specific two-photon imaging of live cellular and deep-tissue lipid droplets by lipophilic AIEgens at ultralow concentration. *Chem. Mater.* **2018**, *30*, 4778−4787.
(44) Cai, Y.; Gui, C.; Samedov, K.; Su, H.; Gu, X.; Li, S.; Luo, W.; Sung, H. H.; Lam, J. W.; Kwok, R. T.; Williams, I. D.; Qin, A.; Tang, B. Z. An acidic pH independent piperazine−TPE AIEgen as a unique bioprobe for lysosome tracing. *Chem. Sci.* **2017**, *8*, 7593−7603.
(45) Li, Y.; Wu, Y.; Chang, J.; Chen, M.; Liu, R.; Li, F. A bioprobe based on aggregation induced emission (AIE) for cell membrane tracking. *Chem. Commun.* **2013**, *49*, 11335−11337.
(46) Chris, Y. Y.; Zhang, W.; Kwok, R. T.; Leung, C. W.; Lam, J. W.; Tang, B. Z. A photostable AIEgen for nucleolus and mitochondria imaging with organelle-specific emission. *J. Mater. Chem. B* **2016**, *4*, 2614−2619.
(47) Ingle, J.; Sengupta, P.; Basu, S. Illuminating Sub-Cellular Organelles by Small Molecule AIEgens. *ChemBioChem* **2023**, *24*, No. e202200370.
(48) Patil, S.; Pandey, S.; Singh, A.; Radhakrishna, M.; Basu, S. Hydrazide−hydrazone small molecules as AIEgens: Illuminating mitochondria in cancer cells. *Chem.—Eur. J.* **2019**, *25*, 8229−8235.
(49) Ingle, J.; Das, B.; Chaudhary, K.; Mondal, A.; Basu, S. Small Molecule AIEgens for Illuminating Sub-Cellular Endoplasmic Reticulum, Mitochondria, and Lysosomes. *ChemBioChem* **2023**, *24*, No. e202300379.
(50) Ingle, J.; Dedaniya, H.; Mayya, C.; Mondal, A.; Bhatia, D.; Basu, S. γ-Resorcyclic Acid-Based AIEgens for Illuminating Endoplasmic Reticulum. *Chem.—Eur. J.* **2022**, *28*, No. e202200203.
(51) Li, J.; Tang, J.; Yang, X.; Xie, P.; Liu, J.; Zhang, D.; Ye, Y. A novel aggregation-induced emission fluorescent probe to visualize peroxynitrite levels during Golgi stress. *Sens. Actuators B: Chem.* **2022**, *358*, No. 131513.
(52) Wang, X.; Wang, X.; Li, Y.; Qi, Z. COX-2 inhibition mediated aggregation-induced emission photosensitizer target the Golgi apparatus for selective imaging of cancer cells and enhanced photodynamic therapy. *Dyes Pigm.* **2024**, *222*, No. 111897.
(53) Liu, M.; Chen, Y.; Guo, Y.; Yuan, H.; Cui, T.; Yao, S.; Jin, S.; Fan, H.; Wang, C.; Xie, R.; He, W. Golgi apparatus-targeted aggregation-induced emission luminogens for effective cancer photodynamic therapy. *Nat. Commun.* **2022**, *13*, 2179.
(54) Xiao, P.; Ma, K.; Kang, M.; Huang, L.; Wu, Q.; Song, N.; Ge, J.; Li, D.; Dong, J.; Wang, L.; Wang, D. An aggregation-induced emission platform for efficient Golgi apparatus and endoplasmic reticulum specific imaging. *Chem. Sci.* **2021**, *12*, 13949−13957.
(55) Luo, Y.; Zhang, S.; Wang, H.; Luo, Q.; Xie, Z.; Xu, B.; Tian, W. Precise detection and visualization of cyclooxygenase-2 for Golgi imaging by a light-up aggregation-induced emission-based probe. *Ccs Chemistry.* **2022**, *4*, 456−463.
(56) Henwood, A. F.; Curtin, N.; Estalayo-Adrián, S.; Savyasachi, A. J.; Gudmundsson, T. A.; Lovitt, J. I.; Sigurvinsson, L. C.; Dalton, H. L.; Hawes, C. S.; Jacquemin, D.; O'Shea, D. F. Time-resolved fluorescence imaging with color-changing,"turn-on/turn-on" AIE nanoparticles. *Chem* **2024**, *10*, 578−599.
(57) Sanyam; Khatua, R.; Mondal, A. Constructing Multiresonance Thermally Activated Delayed Fluorescence Emitters for Organic LEDs: A Computational Investigation. *J. Phys. Chem. A* **2023**, *127*, 10393−10405.
(58) Sanyam; Khatua, R.; Mondal, A. Cost-Effective Approach for Modeling of Multiresonant Thermally Activated Delayed Fluorescence Emitters. *J. Chem. Theory Comput.* **2023**, *19*, 9290−9301.
(59) Sanyam; Sorout, P.; Mondal, A. Rational Design of Organic Emitters with Inverted Singlet−Triplet Gaps for Enhanced Exciton Management. *J. Phys. Chem. A* **2024**, *128*, 7114−7123.
(60) Tan, W.; Zhang, Q.; Quiñones-Frías, M. C.; Hsu, A. Y.; Zhang, Y.; Rodal, A.; Hong, P.; Luo, H. R.; Xu, B. Enzyme-responsive peptide thioesters for targeting Golgi apparatus. *J. Am. Chem. Soc.* **2022**, *144*, 6709−6713.
(61) Orci, L.; Stamnes, M.; Ravazzola, M.; Amherdt, M.; Perrelet, A.; Söllner, T. H.; Rothman, J. E. Bidirectional transport by distinct populations of COPI-coated vesicles. *Cell* **1997**, *90*, 335−349.
(62) Spang, A. Retrograde traffic from the Golgi to the endoplasmic reticulum. *Cold Spring Harb Perspect Biol.* **2013**, *5*, No. a013391.

https://doi.org/10.1021/acsabm.4c01722
ACS Appl. Bio Mater. XXXX, XXX, XXX−XXX